Title
Properties of photon density waves in multiple-scattering media.

Journal
Applied Optics, 32(4)

ISSN
0003-6935

Authors
Tromberg, Bruce J
Svaasand, Lars O
Tsay, Tsong-Tseh
et al.

Publication Date
1993-02-01

DOI
10.1364/ao.32.000607

Properties of photon density waves in multiple-scattering media

Bruce J. Tromberg, Lars O. Svaasand, Tsong-Tseh Tsay, and Richard C. Haskell

Amplitude-modulated light launched into multiple-scattering media, e.g., tissue, results in the propagation of density waves of diffuse photons. Photon density wave characteristics in turn depend on modulation frequency (ω) and media optical properties. The damped spherical wave solutions to the homogeneous form of the diffusion equation suggest two distinct regimes of behavior: (1) a high-frequency dispersion regime where density wave phase velocity V_p has a $\sqrt{\omega}$ dependence and (2) a low-frequency domain where V_p is frequency independent. Optical properties are determined for various tissue phantoms by fitting the recorded phase (ϕ) and modulation (m) response to simple relations for the appropriate regime. Our results indicate that reliable estimates of tissuelike optical properties can be obtained, particularly when multiple modulation frequencies are employed.

Key words: Photon density waves, frequency-domain photon migration, tissue optical properties, multiple-scattering media.

Introduction

Much of the driving force behind recent developments in time-domain tissue optical spectroscopy[1,2] is derived from studies of short-light-pulse propagation in multiple-scattering media.[3,4] In contrast to continuous illumination techniques,[5,6] pulse propagation methods can provide information about the distribution of scatterers and absorbers in a single measurement.[7,8] These optical properties may be used in a variety of therapeutic and diagnostic techniques including imaging tissue structure,[9–12] monitoring physiology,[13–15] and predicting optical dosimetry for laser-based procedures.[16]

The conceptual basis for the time-domain approach generally involves solutions to the radiative transfer equation[17,18] using Monte Carlo simulation[19,20] and diffusion theory approximations.[4,21] Diffusion-based methods provide relatively straightforward analytical expressions that describe the shape of a diffusely reflected or transmitted pulse in terms of the optical properties of the medium.[7] Thus the observed temporal broadening of ultrashort pulses can be mathematically related to the large number of optical paths available in multiple-scattering media. Since the introduction of losses (absorbers) reduces the average path length, absorber-dependent changes in pulse propagation time can be used to calculate absorption coefficients.[7]

Frequency-domain optical methods can be adapted to diffusion theory models in a similar manner. Fishkin *et al.*[22] first suggested that amplitude-modulated light propagates through homogeneous multiple-scattering media as diffuse waves with a coherent front. These photon density waves can be characterized by a phase velocity V_p and modulation wavelength λ_m that are primarily functions of media optical properties. Diffuse wave properties bear no relationship to corresponding electromagnetic wave features, since, in turbid media, phase relationships between optical waves vary in a rapid stochastic manner.

The power and simplicity of frequency-domain methods have been demonstrated by Lakowicz and Bundt[23] who conducted tissue studies using frequencies to 3 GHz and Sevick *et al.*[13] who reported measurements of hemoglobin saturation at a single modulation frequency. More recently Patterson *et al.*[24] derived frequency-domain analytic expressions in semi-infinite media from the Fourier transform of a time-domain relation. In general frequency-domain techniques are real-time recordings, which compared with time-domain methods, place less stringent demands on the bandwidth of the light source and

B. J. Tromberg and T-T. Tsay are with Beckman Laser Institute, University of California, Irvine, Irvine, California 92715; L. O. Svaasand is with the University of Trondheim, 7000 Trondheim, Norway; and R. C. Haskell is with Harvey Mudd College, Claremont, California 91711.

Received 4 February 1992.
0003-6935/93/040607-10$05.00/0.

detector. When laser diodes and photomultiplier tubes are employed, instrumentation costs can be relatively modest. These useful analytical features suggest the necessity for a thorough practical description of frequency-domain measurements.

Previously we extended the diffusion theory model to include photon density wave behavior over a range of modulation frequencies and varying optical properties.[25,26] In this research, we solve analytically the time-dependent diffusion equation in infinite medium conditions for sinusoidally amplitude-modulated waves. Simplifications to our diffusion equation solutions are proposed and confirmed experimentally. In this manner a general model is presented that describes the unique characteristics of photon density waves. Historically this approach has been applied to a variety of physical phenomena including the description of terrestial temperature oscillations.[27] Although this discussion was confined to thermal diffusion in lossless media, it provides an intuitive picture of diffusely propagating density waves and serves as a framework for photon diffusion in lossy tissues.

Theory

Optical power in multiple-scattering media, e.g., tissue, is typically characterized by the quantities φ, the radiant energy fluence rate, and L, the radiance. The radiant energy fluence rate,

$$\varphi = \int_{\Omega=0}^{4\pi} L\mathrm{d}\Omega,$$

is defined as the optical energy flux incident on an infinitesimally small sphere divided by the cross-sectional area of that sphere. Since the integration is taken over all solid angles Ω, the fluence rate is a measure of the total optical flux. The radiance L is the optical energy flux in some direction per unit solid angle per unit area orthogonal to that direction. In a completely isotropic light field, $L = \varphi/(4\pi)$.

When the optical flux is viewed along the axis of a solid angle element $\mathrm{d}\Omega$, the irradiance E gives the flux per unit area orthogonal to this axis and can be expressed as

$$E = \int_{\Omega=0}^{2\pi} L(-\hat{l}\cdot\hat{n})\mathrm{d}\Omega = \pi L = \frac{\varphi}{4}, \tag{1}$$

where $\hat{l}$ and $\hat{n}$ are, respectively, the unit vectors along the axis and the outward unit surface normal to the solid-angle element. As diffuse photons propagate through tissue, the irradiance onto an element of surface, e.g., a detector, will vary with respect to the source location. When the surface normal points toward the source, E is enhanced so that

$$E = \frac{\varphi}{4} + \frac{j}{2}.$$

Similarly, E is reduced when the surface normal points directly away from the source and

$$E = \frac{\varphi}{4} - \frac{j}{2}.$$

The magnitude j of the transport vector $\mathbf{j}$ represents the total deviation from a completely isotropic distribution. This deviation is a consequence of the diffusion process since the net transport of diffuse photons in some direction must be expressed by a higher radiance in that direction.

To satisfy the requirements for the directional transport of diffuse photons, the radiance is expressed as a series expansion of the form

$$L = \frac{\varphi}{4\pi} + \alpha\mathbf{j}\cdot\hat{l} + \cdots. \tag{2}$$

The constant α can be determined by combining Eq. (1) with the flux-dependent expression for E:

$$E = \int_{\Omega=0}^{2\pi}\left[\frac{\varphi}{4\pi} + \alpha(\mathbf{j}\cdot\hat{l})\right](-\hat{l}\cdot\hat{n})\mathrm{d}\Omega = \frac{\varphi}{4} + \frac{2\pi\alpha}{3}j, \tag{3}$$

thus yielding $\alpha = 3/4\pi$. Substituting into Eq. (2) results in the radiance series expansion[21]:

$$L = \frac{\varphi}{4\pi} + \frac{3}{4\pi}\mathbf{j}\cdot\hat{l} + \cdots, \tag{4}$$

where the term $\varphi/4\pi$ corresponds to a completely isotropic distribution and $[3/(4\pi)]\mathbf{j}\cdot\hat{l}$ represents the net transport of diffuse photons.

The migration of diffuse photons proceeds from regions of high to low fluence rate and can be expressed by Fick's law:

$$\mathbf{j} = -\zeta\,\mathrm{grad}\,\varphi, \tag{5}$$

where ζ, the photon diffusion constant, is a composite function of the scattering σ and absorption, β, coefficients[21]:

$$\zeta = \frac{1}{3[\sigma(1-g)+\beta]} = \frac{1}{3(\sigma_{\mathrm{eff}}+\beta)}, \tag{6}$$

and the effective scattering coefficient σ_{eff} is determined by the average cosine of the scattering angle g. To satisfy the diffusion approximation, $\sigma_{\mathrm{eff}} \gg \beta$.

For diffuse photons migrating out of a unit volume, the net flux is characterized by

$$\mathrm{div}\,\mathbf{j} = -\frac{1}{c}\frac{\partial\varphi}{\partial t} - \beta\varphi + q. \tag{7}$$

Equations (5) and (7) can then be combined to yield the time-dependent diffusion equation[7,28]

$$X\nabla^2\varphi - \frac{\partial\varphi}{\partial t} - \frac{\varphi}{\tau} = -qc, \tag{8}$$

where c is the velocity of light in the medium (we assume throughout that $n \approx 1.33$ for tissue phantom fat emulsions; therefore $c \approx 2.26 \times 10^8$ m/s), q is the source term for the rate of photon generation per unit volume, $X = \zeta c$ is the optical diffusivity, and $\tau = 1/\beta c$ is the optical absorption relaxation time.

The homogeneous form of Eq. (8) (i.e., $q = 0$) can be employed[7] and solved analytically for three-dimensional harmonic waves of the form

$$\varphi(\mathbf{r}, t) = \varphi_0 \frac{\exp(-r/\delta)}{r} + \varphi_1 \frac{\exp(k_r r)}{r} \exp[i(k_i r - \omega t)], \tag{9}$$

where the first and second terms on the right-hand side of Eq. (9) are, respectively, the time-independent (dc) and time-dependent (ac) components of a spatially r and temporally t varying source rate $\varphi(\mathbf{r}, t)$, ω is the angular modulation frequency, and k_r and k_i are the real and imaginary components of the complex angular wave number k (k_r is attenuation and k_i is the phase per unit length). The dc penetration depth is given by $\delta = 1/[3\beta(\beta + \sigma_{\text{eff}})]^{1/2} = (X\tau)^{1/2}$, and the photon density wave phase velocity V_p and modulation wavelength λ_m are by definition

$$\lambda_m = 2\pi/k_i, \tag{10}$$

$$V_p = \omega/k_i. \tag{11}$$

These parameters describe the collective properties of diffuse density waves, not individual photons. Specifically λ_m and V_p are, respectively, measures of the minimum distance in space between regions with the same phase of diffuse photon density and phase-front propagation velocity.

The infinite-medium solutions to Eq. (8) can be expressed in terms of the complex wave number[29]:

$$k_r = \frac{1}{(2X\tau)^{1/2}} \{[1 + (\omega\tau)^2]^{1/2} + 1\}^{1/2}, \tag{12}$$

$$k_i = \frac{1}{(2X\tau)^{1/2}} \{[1 + (\omega\tau)^2]^{1/2} - 1\}^{1/2}. \tag{13}$$

These relations are illustrated in Fig. 1. Although specific tissuelike optical properties ($X = 1.5 \times 10^4$ m^2/s and $\tau = 0.44$ ns) were selected for the Fig. 1 simulation, the general appearance of ω versus k curves is independent of optical properties. Changes in X and τ simply alter the extent of the high- and low-frequency regimes.

For example, in the high-frequency dispersion regime, $\omega \gg 1/\tau$ and $k_r \approx k_i \approx [\omega/(2X)]^{1/2}$. In these conditions density wave properties are dominated by scattering. They are heavily damped with a constant $\exp(-2\pi r/\lambda m)$ attenuation; thus the amplitude is reduced to 0.19% of its initial value over a distance

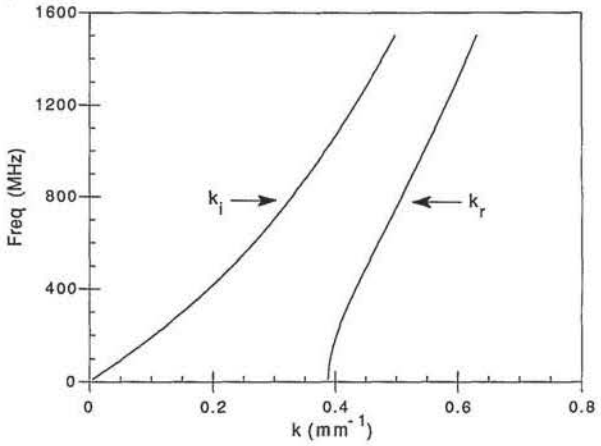

Fig. 1. Theoretical frequency (MHz) versus k (mm^{-1}) response derived from analytical solutions to Eq. (8) for the following optical properties: $\tau = 0.44$ ns, $\sigma_{\text{eff}} = 50$ cm^{-1}, and $X = 1500$ m^2/s.

of λ_m. The corresponding phase velocity is given by

$$V_p = \omega/k_i = (2X\omega)^{1/2}, \tag{14}$$

and V_p is proportional to $\sqrt{\omega}$. As the modulation frequency is reduced, light is collected from larger regions and phase velocity decreases. This behavior continues until V_p is independent of the modulation frequency ($\omega \ll 1/\tau$), and wave properties are dominated by absorption (see below).

At higher frequencies there is greater attenuation and light is collected from smaller regions. The time required to achieve a steady-state photon distribution is reduced and V_p increases with $\sqrt{\omega}$. Multiple scattering cannot occur, however, when the modulation frequency is greater than the reciprocal of the average time between scattering events, i.e., $\omega \ll c\sigma_{\text{eff}} = 1/\tau_{sc}$. Since the validity of diffusion theory is based on multiple scattering, the upper frequency limit to diffusion theory is imposed by the scattering relaxation time τ_{sc}. In tissues with $\sigma_{\text{eff}} \approx 50$ cm^{-1}, this corresponds to ~ 180 GHz.

In contrast to dispersion-regime behavior, the properties of low-frequency waves are dominated by absorption. Low-frequency ($\omega \ll 1/\tau$) phase velocity reaches a dispersionless lower limit independent of modulation frequency. The solutions for k reduce to

$$k_i \approx \frac{\omega\tau}{2(X\tau)^{1/2}}, \tag{15}$$

$$k_r \approx \frac{1}{(X\tau)^{1/2}} = 1/\delta, \tag{16}$$

and $V_p = 2(X/\tau)^{1/2}$. In Fig. 1 the onset of this behavior would occur at modulation frequencies that are well below $\omega = \beta c$ (i.e., 360 MHz). When ω is particularly small with respect to $1/\tau$, the ac and dc attenuation rates are equal. Figure 1 clearly illustrates this frequency-independent region where k_r approaches the reciprocal of the dc penetration depth

δ. As ω increases, however, some frequency dependence can be observed. Provided that $\omega\tau < 0.7$, expanding k_r in powers of ωτ and keeping the leading term yield

$$k_r = \frac{1}{(X\tau)^{1/2}} \times \left[1 + \frac{(\omega\tau)^2}{8} + \cdots\right]. \quad (17)$$

Thus the dispersionless attenuation ranges from a frequency-independent limit where $k_r \approx 1/\delta$ to an upper boundary where $k_r \propto 1 + [(\omega\tau)^2/8]$.

Frequency-domain measurements record phase lag(ϕ) and demodulation amplitude m with respect to a source response. Since these parameters can be defined in terms of the complex wave number, ϕ and m are simply functions of ω, r, and the optical properties τ and σ_{eff}:

$$\phi = k_i r = r\{\beta[\beta + (1-g)\sigma]\}^{1/2}\left(\frac{3}{2}\right)^{1/2} \times \left\{\left[1 + \left(\frac{\omega}{\beta c}\right)^2\right]^{1/2} - 1\right\}^{1/2}, \quad (18)$$

$$m = \frac{(ac/dc)_{sample}}{(ac/dc)_{source}} = \frac{\left\{\varphi_1 \dfrac{\exp(-k_r r)}{r} \Big/ \varphi_0 \dfrac{\exp[-r/(X\tau)^{1/2}]}{r}\right\}}{(\varphi_1/\varphi_0)_{r=0}} = \exp\left[-\left(k_r - \frac{1}{\delta}\right) r\right]. \quad (19)$$

therefore

$$-\ln(m) = r\{\beta[\beta + (1-g)\sigma]\}^{1/2}\left(\frac{3}{2}\right)^{1/2} \times \left(\left\{\left[1 + \left(\frac{\omega}{\beta c}\right)^2\right]^{1/2} + 1\right\}^{1/2} - \sqrt{2}\right). \quad (20)$$

Materials and Methods

Instrumentation

The photon migration instrument is a modified multiharmonic Fourier transform phase and modulation fluorometer (SLM, Model 48000-MHF, Champaign, Ill.) illustrated in Fig. 2. Light (L) is provided either by a water-cooled argon-ion laser (Innova 90-5, Coherent, Palo Alto, Calif.) or an argon-pumped dye laser (Coherent Model 599) with DCM dye (Exciton, Inc., Dayton, Ohio). A Pockels cell (PC), driven either directly by a frequency synthesizer or indirectly by the amplified output of a harmonic comb generator (HCG), is used to modulate light at single frequencies or produce pulses with high harmonic content (multiharmonic mode).

In multiharmonic operation, phase and modulation data from 50 frequencies, up to 250 MHz, can be acquired in a few seconds.[30] The three harmonic comb generators (HCG1, HCG2, HCG3) receive inputs from a frequency source FG at 5 and 5 MHz + 3 Hz. The comb generator outputs are, in the time domain, an impulse with a 5-MHz repetition rate and, in the frequency domain, a fundamental frequency (5 MHz) and its integer harmonics, 5, 10, 15 MHz, etc. The impulse from HCG1 is amplified and applied to the Pockels cell. This produces a pulse of light with high harmonic content, which is focused onto a 600-μm-diam fused-silica fiber-optic probe (F1). A small portion of this light is diverted to a reference photomultiplier tube (PMTr) (Hammatsu R928), which allows phase and modulation locking of the instrument. The optical fiber is used to direct the bulk of the light into the sample, and a second fiber (F2) collects the scattered light.

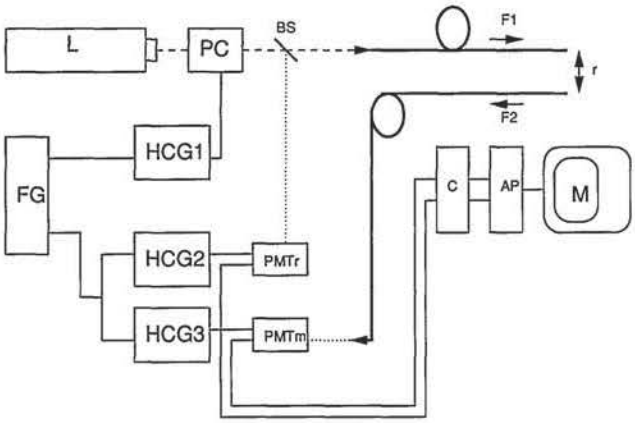

Fig. 2. Frequency-domain instrument (see text for a detailed description). BS, beam splitter; M, display monitor; r, distance.

Scattered light is transmitted by F2 to the measurement photomultiplier tube (PMTm) (Hammatsu R928). The gain of the photomultiplier tubes is modulated by HCG2 and HCG3. Since the output of these devices are the harmonic combs, 5 MHz + 3 Hz, 10 MHz + 6 Hz, 15 MHz + 9 Hz, etc., the sample's phase and amplitude response at each harmonic is contained within the cross-correlation frequencies, 3, 6, 9, Hz etc. These 3-Hz cross-correlation notes are sampled and digitized by a dual-channel analog-to-digital converter (C). An array processor (AP) performs the transform that converts the digital data to a frequency spectrum ranging from 3 to ~150 Hz. Phase and modulation information from the high-frequency components of the harmonic comb function (5 . . . 250 MHz) is contained within the 3- . . . 150-Hz spectrum. Phase and modulation values are computed from the real and imaginary components of the transforms.

Single-frequency readings are acquired simply by eliminating the HCG circuit and tuning the frequency synthesizers to the region of interest. Reference/sample measurements are interleaved, and, as above, cross-correlation detection[31] is employed.

Materials

All scattering measurements were conducted in a 30 × 30-cm black-walled cylindrical vessel filled with 10 L of an emulsified fat solution, Intralipid (KabiVitrum, Inc., Clayton, N.C.). Fibers (flat-cut faces,

600-μm core diameter) were positioned in the center of the liquid, parallel to each other. This central location was selected carefully to simulate an infinite medium. The distance between the source and collection fibers was systematically varied between 5 and 20 mm for each measurement series. Reference (i.e., source) measurements were recorded in air with input and collection fibers facing each other.

A porphyrin compound, tetraphenyl porphine tetrasulfonate ($TPPS_4$) (Porphyrin Products, Logan, Ut.) was added to the Intralipid so the effect of the absorber could be quantitatively determined. A 514-nm laser-line filter (Corion Corporation, Holliston, Mass.) was placed at the entrance to the PMT housing to block $TPPS_4$ fluorescence and isolate the scattered light.

Results and Discussion

Figure 3 illustrates the distance dependence for phase (Figs. 3A and 3B) and modulation (Figs. 3B and 3D) predicted by Eqs. (18) and (20). Data are presented for various frequencies between 5 and 200 MHz in 2% Intralipid ($\lambda = 650$ nm). As can be seen in Figs. 3A and 3B, the frequency response is predominantly nonlinear regardless of distance. This implies density wave dispersion over most of the modulation region. Furthermore small changes in fiber separation substantially influence phase and modulation values.

Redisplaying ϕ and $-\ln(m)$ as a function of distance clearly demonstrates the predicted linear relationship for all frequencies (Figs. 3C and 3D). Higher frequencies result in shorter modulation wavelengths or more photon density fluctuations per unit distance. Attenuation and phase lag increase as the modulation wavelength is reduced; thus an increase in k, ϕ, and $-\ln(m)$ are observed. As expected the distance linearity is maintained regardless of whether density waves fall within the dispersion or nondispersion regimes.

In Fig. 4 phase and modulation are shown as a function of frequency for fibers placed 1.0 cm apart in 0.4%, 2%, and 10% Intralipid ($\lambda = 650$ nm). The smooth curves through the data represent the best nonlinear least-squares fits to Eqs. (18) and (20). Values for β and σ_{eff} can be calculated by using either Eq. (18) or (20), provided that there is sufficient nonlinearity (i.e., substantial dispersion behavior) for reliable fits.

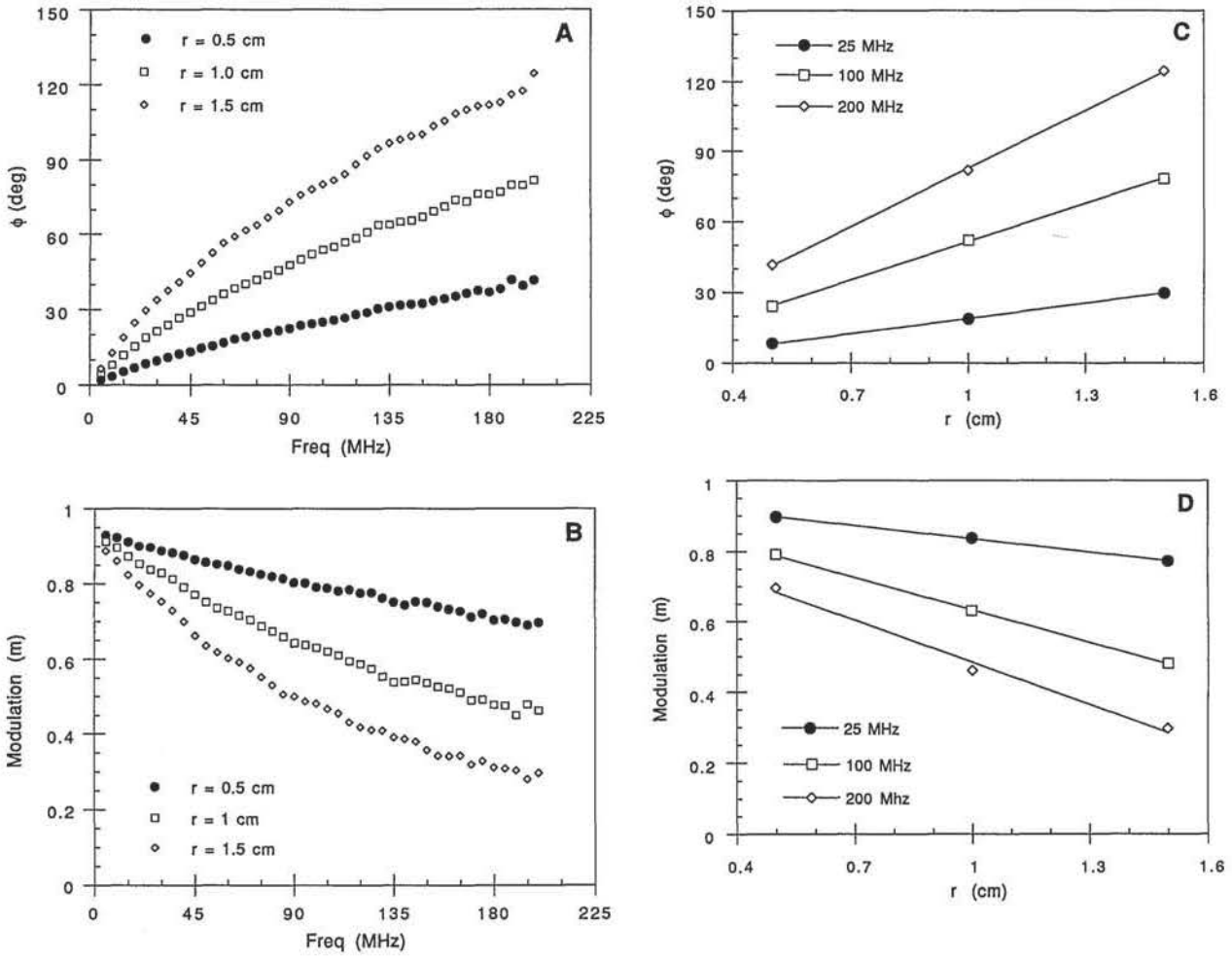

Fig. 3. (A) Phase and (B) modulation versus frequency (5–200 MHz) for various values of r. Linear fits to (C) phase and (D) modulation versus r for selected frequencies (25, 100, 200 MHz). Measurements in 2% Intralipid; $\lambda = 650$ nm; $r = 0.5$, 1.0, and 1.5 cm.

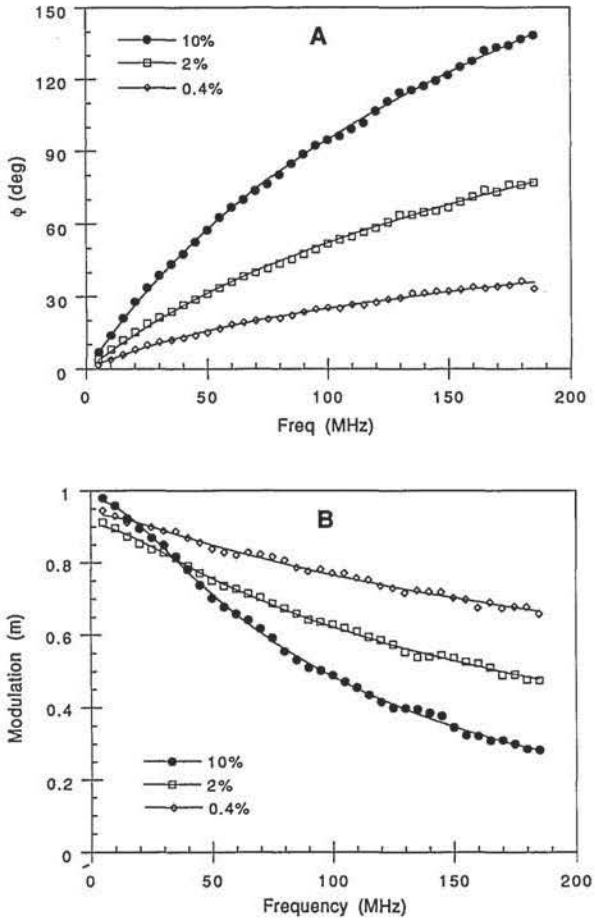

Fig. 4. (A) Phase and (B) modulation versus frequency for 10%, 2%, and 0.4% Intralipid; $\lambda = 650$ nm, $r = 1.0$ cm. Smooth curves through the data represent the best nonlinear least-squares fits to Eqs. (18) and (20).

Optical properties derived from this method are displayed in Fig. 5 and summarized in Table 1. Each β and σ_{eff} value is an average of phase and modulation estimates at three fiber distances. Figure 5 clearly illustrates that β is relatively insensitive to changes in scattering solution concentration; however, five-fold Intralipid dilutions result in commensurate σ_{eff} reductions.

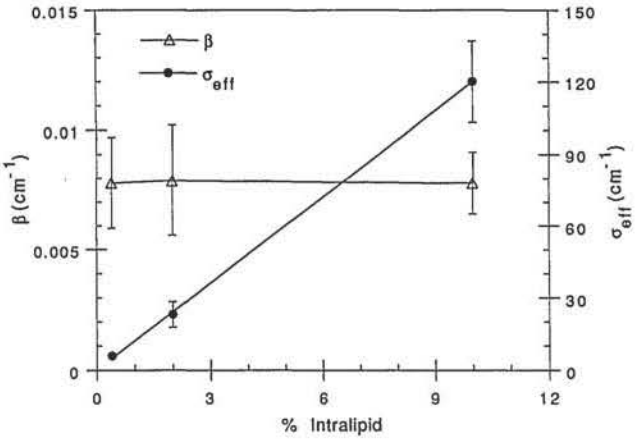

Fig. 5. Summary of optical property measurements in 10%, 2%, and 0.4% Intralipid estimated from nonlinear phase and modulation fits. σ_{eff} is linearly proportional to and β is independent of % Intralipid. All measurements were made at $\lambda = 650$ nm; $r = 0.5$, 1.0, and 1.5 cm.

Table 1. Calculated Absorption β and Effective Scattering σ_{eff} Coefficients for 0.4%. 2%, and 10% Intralipid Solutions

Intralipid (%)	β (cm^{-1})	σ_{eff} (cm^{-1})
0.4	0.0078 ± 0.0019	5.8 ± 0.54
2	0.0079 ± 0.0023	23 ± 5.3
10	0.0078 ± 0.0013	120 ± 17

Note: Values are averages of six separate measurements, i.e., phase and modulation full fits at three source–detector distances.

The full-fit results obtained from Fig. 4 suggest that the linear-frequency region ($\omega\tau < 0.7$) for 10%, 2%, and 0.4% Intralipid should be <20 MHz. In these low-frequency conditions the solutions for k, given by Eqs. (15) and (17), yield the following expressions for ϕ and m:

$$\phi = k_i r \approx \frac{\left(\frac{3}{2}\sigma_{eff}\right)^{1/2}}{c(2\beta)^{1/2}} \times r\omega, \tag{21}$$

$$-\ln(m) = \left[k_r - \frac{1}{(X\tau)^{1/2}}\right] \times r \approx \frac{\left(\frac{3}{2}\sigma_{eff}\right)^{1/2}}{c(2\beta)^{1/2}} \times \frac{r\omega^2}{4\beta c}. \tag{22}$$

Linear fits to ϕ versus ω and $-\ln(m)$ versus ω^2 furnish constant slopes, m_ϕ and $m_{-\ln(m)}$, respectively, which can be used to calculate β (independent of r):

$$\beta = \frac{m_\phi}{4c \times m_{-\ln(m)}}. \tag{23}$$

Linear-fit β values obtained from 5-, 10-, 15-, and 20-MHz data at six different source–detector distances are summarized in Table 2. These results are in reasonable agreement with full-fit β values; however, since only a few frequencies were available to satisfy $\omega\tau < 0.7$, full-fit methods should be more accurate. For example, assuming that the reported 0.4% Intralipid-β is accurate, rigorous fulfillment of the $\omega\tau < 0.7$ criterion would require an upper-frequency limit of only 13 MHz. The superior linear-fit precision is also a consequence of the limited number of modulation frequencies. Extremely low absorption coefficients are calculated from small values of m_ϕ and $m_{-\ln(m)}$, which in turn are determined

Table 2. Absorption Coefficients and Frequency-Independent Phase Velocities Determined from Low-Frequency Data Where $\omega\tau < 0.7$

Intralipid (%)	β (cm^{-1})[a]	V_p (cm/s)
0.4	0.0040 ± 0.00018	7.61×10^8
2	0.0050 ± 0.00022	3.74×10^8
10	0.0074 ± 0.00051	1.73×10^8

[a]Values of β are averages of six source–detector distances.

from close to the minimum number of points required for a straight line. Thus m_ϕ and $m_{-\ln(m)}$ appear to be precise, when in fact they are determined from too small a data set.

Figure 6A illustrates the low-frequency phase response for each Intralipid dilution ($r = 1$ cm). When this behavior is linear, the phase velocity can be obtained from the distance dependence of m_ϕ displayed in Fig. 6B. The linear appearance of m_ϕ versus r for each Intralipid concentration suggests medium homogeneity. Since $k_i = \phi/r$ [Eq. (18)] and $V_p = \omega/k_i$ [Eq. (11)],

$$m_\phi = \phi/\omega = r/V_p. \tag{24}$$

Thus the reciprocal of the m_ϕ versus r slope (Fig. 6B) yields V_p. This is the lower limit for phase velocity. V_p remains independent of ω up to modulation frequencies where $\omega\tau < 0.7$. In the region where $\omega\tau \approx 1$ (i.e., $0.7 < \omega\tau < 1.4$), k_i is on the edge of the Fig. 1 parabola and V_p begins to display some frequency dependence. For $\omega\tau \gg 1$, V_p assumes the full $(\omega)^{1/2}$ dependence described by Eq. (14). Frequency-independent V_p values are summarized in Table 2. Density wave phase velocities range from as little as $0.0076c$ in 10% Intralipid to a high of only $0.034c$ in 0.4% solution.

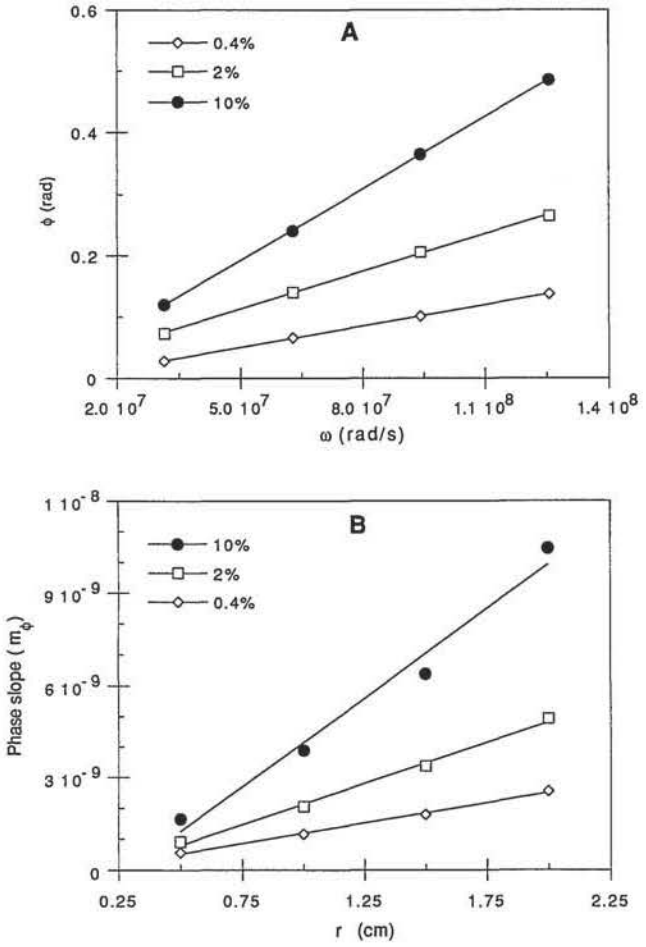

Fig. 6. A, low-frequency phase (rad) versus ω (rad/s) response for $r = 1.0$ cm. The slopes of the linear fits are m_ϕ (see text). B, phase slope (m_ϕ) from A for several fiber separations; the reciprocal of each B slope is the low-frequency phase velocity (see text). Measurements in 10%, 2%, and 0.4% Intralipid; $\lambda = 650$ nm.

Figure 7 illustrates that, for constant absorption, the phase velocity is linearly proportional to $1/\sqrt{\sigma_{\text{eff}}}$. Accordingly a fivefold increase in percent Intralipid results in a $\sqrt{5}$ phase-velocity decrease. V_p reduction in turn leads to shorter modulation wavelengths (λ_m), greater phase lag (ϕ), and enhanced $-\ln(m)$. In practical terms lowering V_p can lead to improved absorber detectability, as illustrated by the concentration-dependent sensitivity improvements of Fig. 6A. However, these exceptionally low phase velocities are rarely observed in real tissues. Despite the scattering similarities between Intralipid and some tissue, absorption differences, typically of an order of magnitude, lead to substantial V_p enhancement *in vivo*.

Figure 8 illustrates the effect of the $TPPS_4$ absorber on phase (Fig. 8A) and modulation (Fig. 8B) in 10% Intralipid ($\lambda = 514$ nm). Modulation frequencies to 165 MHz are shown at a source–detector separation of 7.5 mm. There is distinct nonlinearity to the ϕ and m versus frequency curves in the absence of $TPPS_4$. However, as the absorber is added, the frequency response flattens out. More specifically, phase decreases and attenuation increases [i.e., larger (m) values] with increasing absorber concentration. This occurs because, with the addition of the absorber, measured photons follow shorter paths to the detector. Thus fewer scattering events are recorded, and a decrease in phase delay and demodulation is observed. When the scattering coefficient is held constant, the increasing β results in higher phase velocities ($V_p \propto \sqrt{\beta}$) and longer modulation wavelengths (λ_m).

In high absorption conditions (i.e., when $\omega\tau \ll 1$), m [Eq. (19)] may be close to (or equal to) unity since k_r approaches $1/\delta$. If there is sufficient demodulation to satisfy Eq. (22), β can be determined from Eq. (23). Redisplaying the phase (Fig. 9A) and $-\ln(m)$ (Fig. 9B)

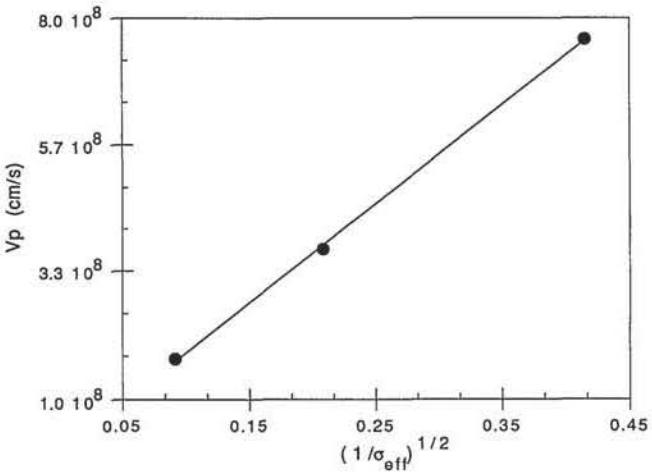

Fig. 7. Phase velocity (determined from Fig. 6B) versus $(1/\sigma_{\text{eff}})^{1/2}$ for 10%, 2%, and 0.4% Intralipid; $\lambda = 650$ nm. The linear relation shown is predicted by diffusion equation solutions.

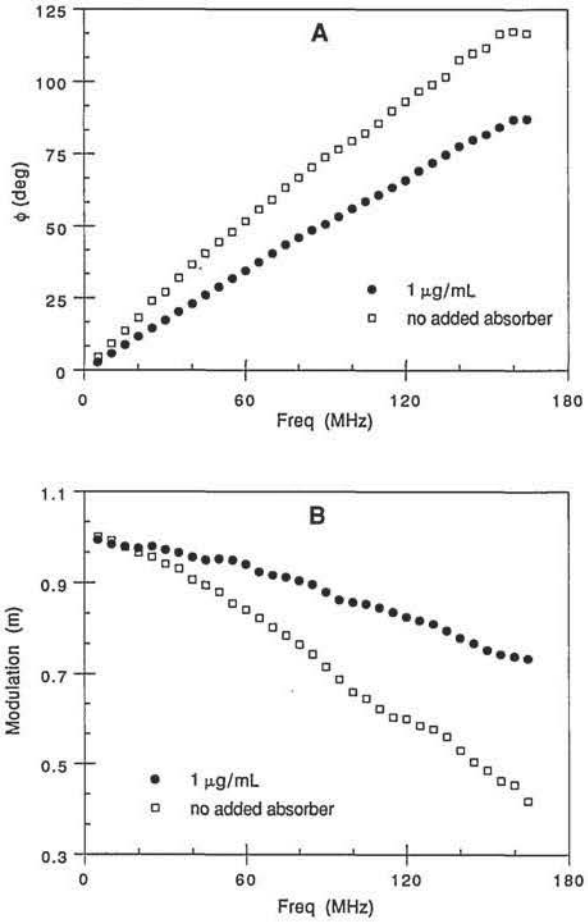

Fig. 8. A, Phase and B, modulation versus frequency response for 10% Intralipid with and without 1 μg/mL of $TPPS_4$ absorber; r = 0.75 cm, λ = 514 nm.

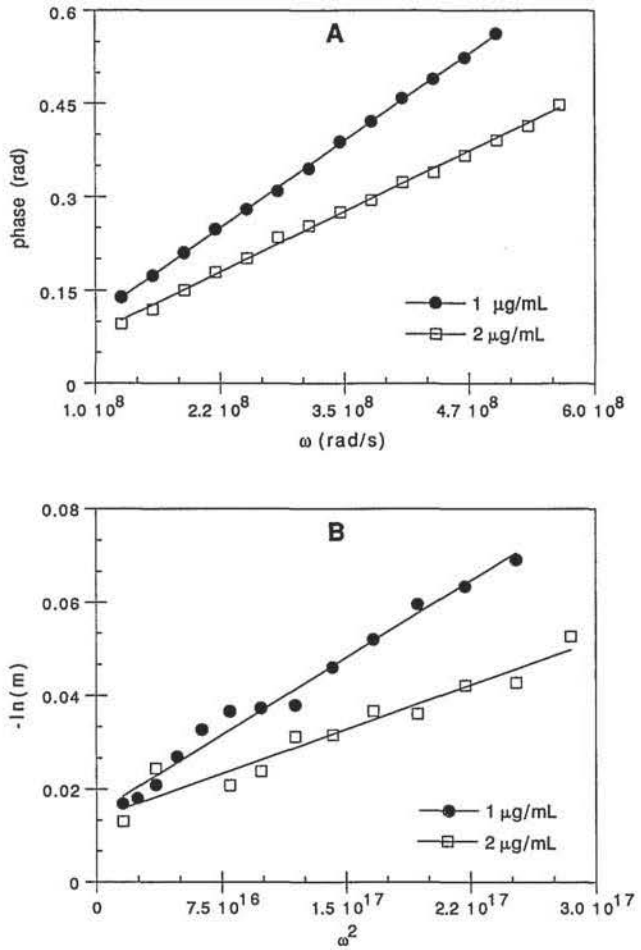

Fig. 9. Best linear fits to A phase versus ω and B $-\ln(m)$ versus ω^2 in the low-frequency regime where $\omega\tau < 0.7$. Measurements in 10% Intralipid with 1 and 2 μg/mL of $TPPS_4$ absorber; r = 0.5 cm, λ = 514 nm.

as functions of ω and ω^2, respectively, illustrates the utility of this linear-fit approach.

Linear-fit absorption coefficients were determined for 1-, 2-, and 4-μg/mL $TPPS_4$ solutions in 10% Intralipid. Nonlinear fits were used to calculate the absorption coefficient of pure 10% Intralipid. Average β values, obtained from at least five separate distance measurements, are displayed as a function of $[TPPS_4]$ in Fig. 10. The molar concentration of $TPPS_4$ in Intralipid can be calculated from the relationship between the linear absorption coefficient β and the molar extinction coefficient ε, i.e., $\beta = 2.3\varepsilon C$, where $\varepsilon(TPPS_4) = 2.5 \times 10^4\ M^{-1}\ cm^{-1}$ at 514 nm. These results, summarized in Table 3, show reasonable agreement between calculated and actual values of concentration.

The linear appearance of Fig. 10 indicates that relatively low β values (0.02 absorbance units, 8×10^{-7} M) can be reliably determined despite the presence of substantial scattering. In fact scattering enhances detectability by slowing V_p and reducing λ_m to dimensions that approach $1/\beta$. Assuming diffusion behavior, the accuracy of high-β determinations is generally limited by signal quality. Most tissue measurements (in the red and near-IR spectral regions) should display some demodulation when accessible frequencies are used, e.g., up to 200 MHz. Unfortunately, as indicated clearly in Fig. 9, the quality of our modulation data is generally poorer

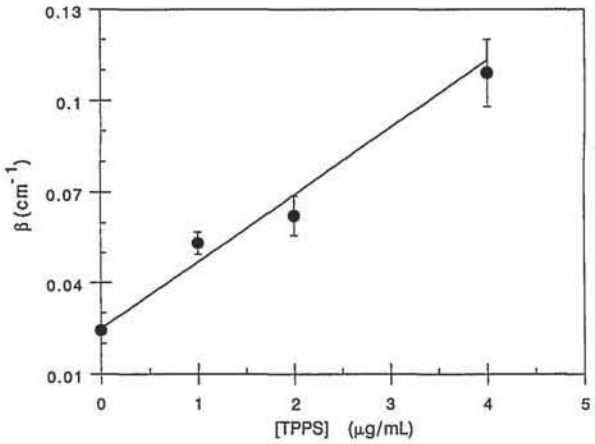

Fig. 10. Absorption coefficient estimated from multifrequency measurements versus concentration of $TPPS_4$ absorber added to 10% Intralipid. Linear regression yields $y = 0.022x + 0.025$, where 0.025 $cm^{-1} = \beta$ in the absence of added absorber; $\chi^2 = 2.17$.

Table 3. Comparison of Actual and Fitted Values of β for $TPPS_4$ in 10% Intralipid, λ = 514 nm

[$TPPS_4$] (μg/mL)	Actual β ($TPPS_4$) cm^{-1}	Fitted β ($TPPS_4$) cm^{-1} [a]
0	0	0
1	0.046	0.047
2	0.092	0.069
4	0.18	0.11

[a]Fitted β were obtained from Fig. 10. Actual $\beta = 2.3\epsilon C$.

than the phase response. As a result the acceptability of $m_{-\ln(m)}$ obtained from linear fits diminishes with increasing β. These factors underscore the importance of acquiring multiple modulation frequencies.

One can employ single-frequency measurements to calculate β by recognizing that $m_\phi = \phi/\omega$ and $m_{-\ln(m)} = -\ln(m)/\omega^2$. Owing primarily to variations in the precision of m, however, the reliability of single-frequency determinations may not be as high as multifrequency calculations. Obviously small variations in $-\ln(m)/\omega^2$ can lead to large errors in the estimation of β; thus it is desirable to acquire ϕ and m for as many frequencies as possible. In addition, by looking at the entire frequency response, one can rapidly determine whether it is appropriate to apply the dispersion relations to calculate optical properties.

This work was performed with support from the University of California Cancer Research Coordinating Committee, The George Hewitt Foundation for Medical Research, the Office of Naval Research grant N00014-91-C-0134, and the Department of Energy grant DE-FG03-91ER61227. The authors thank Khai Vu, Eric Cho, and Matthew McAdams for their outstanding contributions.

References

1. B. Chance, J. Leigh, H. Miyake, D. Smith, S. Nioka, R. Greenfield, M. Finlander, K. Kaufmann, W. Levy, M. Yound, P. Cohen, H. Yodshioka, and R. Boretsky, "Comparison of time-resolved and unresolved measurements of deoxyhemoglobin in brain," Proc. Natl. Acad. Sci. USA **85,** 4971–4975 (1988).
2. D. T. Delpy, M. Cope, P. van de Zee, S. Arridge, S. Wray, and J. Wyatt, "Estimation of optical pathlength through tissue from direct time of flight measurement," Phys. Med. Biol. **33,** 1433–1442 (1988).
3. A. Ishimaru, "Diffusion of a pulse in densely distributed scatterers," J. Opt. Soc. Am. **68,** 1045–1050 (1978).
4. K. Shimizu, A. Ishimaru, L. Reynolds, and A. P. Bruchner, "Backscattering of a picosecond pulse from densely distributed scatterers," Appl. Opt. **18,** 3484–3488 (1979).
5. R. F. Bonner, R. Nossal, S. Havlin, and G. H. Weiss, "Model for photon migration in turbid biological media," J. Opt. Soc. Am. A **4,** 423–432 (1987).
6. R. A. J. Groenhuis, H. A. Ferwerda, and J. J. Ten Bosch, "Scattering and absorption of turbid materials determined by reflection measurements. 1: Theory," Appl. Opt. **22,** 2456–2462 (1983).
7. M. S. Patterson, B. Chance, and B. C. Wilson, "Time-resolved reflectance and transmittance for the noninvasive measurement of tissue optical properties," Appl. Opt. **28,** 2331–2336 (1989).
8. K. M. Yoo and R. R. Alfano, "Determination of the scattering and absorption lengths from the temporal profile of a backscattered pulse," Opt. Lett. **15,** 276–278 (1990).
9. J. R. Singer, F. A. Grunbaum, P. Kohn, and J. P. Zubelli, "Image reconstruction of the interior of bodies that diffuse radiation," Science **248,** 990–993 (1990).
10. R. L. Barbour, H. L. Graber, R. Aronson, and J. Lubowsky, "Imaging of subsurface regions of random media by remote sensing," in *Time-Resolved Spectroscopy and Imaging of Tissues,* B. Chance, ed., Proc. Soc. Photo-Opt. Instrum. Eng. **1431,** 192–203 (1991).
11. D. Benaron, M. A. Lennox, and D. K. Stevenson, "Two-dimensional and 3-D images of thick tissue using time-constrained time-of-flight spectrophotometry," in *Physiological Monitoring and Early Detection Diagnostic Methods,* T. S. Mang, ed., Proc. Soc. Photo-Opt. Instrum. Eng. **1641,** 35–45 (1992).
12. R. Alfano, P.-P. Ho, and K.-M. Yoo, "Photons for prompt tumour detection," Phys. World **5,** 37–40 (1992).
13. E. M. Sevick, B. Chance, J. Leigh, S. Nioka, and M. Maris, "Quantiation of time and frequency-resolved optical spectra for the determination of tissue oxygenation," Anal. Biochem. **195,** 330–351 (1991).
14. B. Chance, S. Nioka, J. Kent, K. McCully, M. Fountain, R. Greenfield, and G. Holtom, "Time-resolved spectroscopy of hemoglobin and myoglobin in resting and ischemic muscle," Anal. Biochem. **174,** 698 (1988).
15. J. M. Schmitt and G.-X. Zhou, "Measurement of blood hematocrit by dual-wavelength near-IR photoplethysmography," in *Physiological Monitoring and Early Detection Diagnostic Methods,* T. S. Mang, ed., Proc. Soc. Photo-Opt. Instrum. Eng. **1641,** 150–161 (1992).
16. S. L. Jacques and S. A. Prahl, "Modeling optical and thermal distributions in tissue during laser irradiation," Lasers Surg. Med. **6,** 494–503 (1987).
17. K. Furutsu, "Diffusion equation derived from space–time transport equation," J. Opt. Soc. Am. **70,** 360–366 (1980).
18. M. S. Patterson, B. C. Wilson, and D. R. Wyman, "The propagation of optical radiation in tissue I. Models of radiation transport and their application," Lasers Med. Sci. **6,** 155–168 (1991).
19. S. L. Jacques, "Time resolved propagation of ultrashort laser pulses within turbid tissues," Appl. Opt. **28,** 2223–2229 (1989).
20. S. T. Flock, M. S. Patterson, B. C. Wilson, and D. R. Wyman, "Monte Carlo modeling of light propagation in scattering tissues—I. Model prediction and comparison with diffusion theory," IEEE Trans. Biomed. Eng. **36,** 1162–1168 (1989).
21. A. Ishimaru, "Diffusion of light in turbid materials," Appl. Opt. **28,** 2210–2215 (1989).
22. J. Fishkin, E. Gratton, M. J. Vande Ven, and W. W. Mantullin, "Diffusion of intensity modulated near-infrared light in turbid media," in *Time-Resolved Spectroscopy and Imaging of Tissues,* B. Chance, ed., Proc. Soc. Photo-Opt. Instrum. Eng. **1431,** 122–135 (1991).
23. J. R. Lakowicz and K. Berndt, "Frequency domain measurements of photon migration in tissues," Chem. Phys. Lett. **166,** 246–252 (1990).
24. M. S. Patterson, J. D. Moulton, B. C. Wilson, K. W. Berndt, and J. R. Lakowicz, "Frequency-domain reflectance for the determination of the scattering and absorption properties of tissue," Appl. Opt. **30,** 4474–4476 (1991).
25. L. O. Svaasand and B. J. Tromberg, "On the properties of optical waves in turbid media," in *Future Trends in Biomedical Applications of Lasers,* L. O. Svaasand, ed., Proc. Soc. Photo-Opt. Instrum. Eng. **1525,** 41–51 (1991).

26. B. J. Tromberg, L. O. Svaasand, T.-T. Tsay, R. C. Haskell, and M. W. Berns, "Optical property measurements in turbid media using frequency domain photon migration," in *Future Trends in Biomedical Applications of Lasers,* L. O. Svaasand, ed., Proc. Soc. Photo-Opt. Instrum. Eng. **1525,** 52–58 (1991).
27. H. S. Carslaw and J. C. Jaeger, *Conduction of Heat in Solids* (Clarendon, Oxford, 1959), pp. 81–83, 272–273.
28. A. Ishimaru, *Wave Propagation and Scattering in Random Media* (Academic, New York, 1978), pp. 175–190.
29. L. O. Svaasand, "Propagation of thermal waves," Med. Phys. **9,** 711–744 (1982).
30. G. W. Mitchell and K. Swift, "A dual-domain Fourier transform fluorescence lifetime spectrofluorometer," in *Time-Resolved Laser Spectroscopy in Biochemistry II,* J. R. Lakowicz, ed., Proc. Soc. Photo-Opt. Instrum. Eng. **1204,** Los Angeles, 270–274 (1990).
31. J. R. Lakowicz, *Principles of Fluorescence Spectroscopy* (Plenum, New York, 1983), p. 78.